Amplitude, Phase, and Quadrant (APQ) Modulation for Indoor Visible Light Communications

Hanaa Abumarshoud[a], Lina Mohjazi[b,*], Sami Muhaidat[c]

[a] *LiFi R&D Centre, University of Strathclyde, Glasgow, United Kingdom*
[b] *School of Engineering, University of Glasgow, Glasgow, United Kingdom*
[c] *Center for Cyber Physical Systems, Department of Electrical and Computer Engineering, Khalifa University, Abu Dhabi, UAE, and Department of Systems and Computer Engineering, Carleton University, Ottawa, Canada*

Abstract

The main challenge in visible light communications (VLC) is the low modulation bandwidth of light-emitting diodes (LEDs). This forms a barrier towards achieving high data rates. Moreover, the implementation of high order modulation schemes is restricted by the requirements of intensity modulation (IM) and direct detection (DD), which demand the use of real unipolar signals. In this paper, we propose a novel amplitude, phase and quadrant (APQ) modulation scheme that fits into the IM/DD restrictions in VLC systems. The proposed scheme decomposes the complex and bipolar symbols of high order modulations into three different symbols that carry the amplitude, phase and quadrant information of the intended symbol. The constructed symbols are assigned different power levels and are transmitted simultaneously, i.e. exploiting the entire bandwidth and time resources. The receiving terminal performs successive interference cancellation to extract and decode the three different symbols, and then uses them to decide the intended complex bipolar symbol. We evaluate the performance of the proposed APQ scheme in terms of symbol-error-rate and achievable system throughput for different setup scenarios. The obtained results are compared with generalized spatial shift keying (GSSK). The presented re-

*Corresponding author
[1] Email addresses:
hanaa.abumarshoud@strath.ac.uk, l.mohjazi@ieee.org, muhaidat@ieee.org.

sults show that APQ offers a higher reliability compared to GSSK across the simulation area, while providing lower hardware complexity.

Keywords: Visible light communications, optical communications, intensity modulation, high order modulation, symbol-error-rate, throughput.

---

1. Introduction

The ever increasing demand for high-speed wireless data connectivity has motivated researchers to look beyond the conventional radio frequency (RF) communications. As a result, the wireless communication industry started moving toward using the radio spectrum above 10 GHz, i.e., mmWave communications, to cope with the influx in data traffic. However, the increase in path loss at such high frequencies necessitates the employment of small cells with strong line-of-sight (LOS) paths. Nevertheless, it is a challenging task to provide backhaul infrastructures to support the deployment of mmWave small cells.

Visible light communication (VLC) has emerged as a promising candidate to support and complement conventional RF communications. Specifically, VLC uses light-emitting diodes (LEDs) as small cells to provide wireless connectivity to a small number of users over a short distance of a few meters. To this end, the intensity of the LED transmitted light is modulated to convey the information signal. This process is known as intensity modulation (IM). At the receiving terminal, a photo detector (PD) is employed to perform direct detection (DD) by translating the fluctuations in the received light intensity into an electrical current that is used for data demodulation. The requirements for the modification of existing lighting infrastructure to support VLC are far simpler and cheaper than the deployment of new infrastructure to support new communication standards. Hence, VLC is considered a potential compelling technology for supporting conventional RF communications [1]. Huge research interests have been directed towards the integration of VLC systems in heterogeneous networks for ubiquitous connectivity. In this regards, VLC can offer exceptionally high

data rates [2], highly secure communications [3] and seamless multi-user access [4]. However, the realization of the full potentials of VLC is subject to its ability to provide sufficiently high data rates, this is particularly crucial due to the following factors: 1) the limited modulation bandwidth of the currently used phosphorescent white LEDs, which spans a few MHz, and 2) the constraints of IM/DD that require the transmitted signal to be positive and real, hindering the implementation of high order modulation schemes. Consequently, the deployment of high spectral efficiency modulation techniques that fit into the constraints of IM/DD is critical in the design of high data-rates VLC systems.

Various high spectral efficiency modulation techniques have been proposed for VLC. For instance, multi-carrier modulation by means of orthogonal frequency-division multiplexing (OFDM) has been widely considered for downlink VLC systems [5, 6]. Since OFDM signals are inherently bipolar and complex, modifications to the conventional OFDM technique are needed to fit into the constraints of IM/DD. To satisfy the reality constraint, Hermitian symmetry is applied on the parallel data streams into the IFFT input in OFDM modules, leading to a spectral loss of half of the available bandwidth. Moreover, to satisfy the non-negativity constraint, a DC bias is added to the generated multicarrier waveform, leading to higher peak-to-average power ratio and increased sensitivity to the LED non-linearity. Several approaches have been proposed for reducing the required DC bias in VLC OFDM systems, including DC-clipped OFDM (DCO-OFDM) [7, 8, 9, 10], asymmetrically clipped optical OFDM (ACO-OFDM)[11, 12], asymmetrically clipped DC biased optical OFDM (ADO-OFDM) [13] and Unipolar OFDM (U-OFDM) [14]. Nevertheless, such modifications come at the cost of additional processing complexity [15].

Space shift keying (SSK) has been proposed as a low complexity modulation technique that is less prone to the LED non-linearity compared to OFDM. SSK is a multiple-input technique which uses the spatial dimension to transmit data [16]. In conventional SSK, only one transmitting LED is activated at any symbol duration, such that the spatial position of the transmitting LED determines the

transmitted symbol [17]. The spectral efficiency of SSK has been improved by proposing generalized SSK (GSSK) [18, 19]. In this scheme, more than one transmitting LEDs are activated at any symbol duration, such that 2^{N_T} possible combinations of transmitters are used to generate a spatial symbol of N_T bits, where N_T denotes the total number of LEDs. The performance of GSSK, however, is highly dependent on the dissimilarity among the channel gains of different receivers. This requirement forms a major limitation of the technique, specifically because of the symmetrical nature of the VLC channel [20].

In this work, we propose a novel optical modulation scheme that we call amplitude, phase, and quadrant (APQ) modulation. The proposed APQ technique can be used to transmit high-order modulation signals via a single transmitting LED and a single PD. This is done by converting the high-order complex constellation symbols into three different components that carry the amplitude, phase and quadrant information of the symbol. Each of the three components is represented by a unipolar pulse-amplitude modulation (PAM) signal of a suitable order. The three signals are then superimposed in the power domain and sent simultaneously. The receiving terminal performs successive interference cancellation (SIC) to decode and separate the three signals and uses the amplitude, phase and quadrant components to constitute the complex symbol.

The remainder of the paper is organized as follows: Section 2 describes the channel and system model of an indoor VLC downlink network. Section 5 presents the benchmark model used for comparison and evaluation. Numerical results and related discussions are presented in Section 6, while closing remarks are provided in Section 7.

2. Channel and System Model

We consider an indoor downlink VLC system realized by a LOS communication link as shown in Fig. 1. The channel gain between the transmitting LED

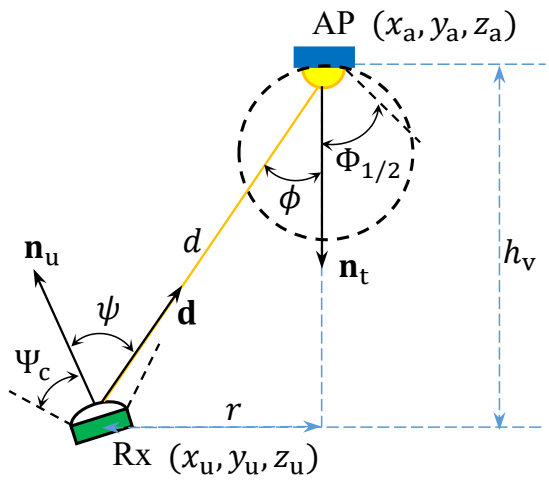

Figure 1: LOS propagation model.

and the receiving PD is given by

$$h = \frac{(m+1)A}{2\pi d^2} \cos^m \phi \; g_f g(\psi) \cos\psi \; \text{rect}\left(\frac{\psi}{\Psi_c}\right), \tag{1}$$

where d is the Euclidean distance between the UE and the AP; A is the physical area of the detector; ϕ and ψ are the angle of radiance with respect to the axis normal to the AP plane, and the angle of incidence with respect to the axis normal to the receiver plane, respectively. Furthermore, $\text{rect}(\frac{\psi}{\Psi_c}) = 1$ for $0 \leq \psi \leq \Psi_c$ and 0 otherwise. The gain of the optical filter is denoted by g_f, and Ψ_c is the receiver field of view (FOV). The optical concentrator, $g(\psi)$, is given as:

$$g(\psi) = \begin{cases} \dfrac{\varsigma^2}{\sin^2 \Psi_c}, & 0 \leq \psi \leq \Psi_c \\ 0, & \text{o.w} \end{cases}, \tag{2}$$

where ς stands for the refractive index; and also m is the Lambertian order which is:

$$m = -\frac{1}{\log_2(\cos \Phi_{1/2})}, \tag{3}$$

where $\Phi_{1/2}$ is the half-intensity angle [21]. The radiance angle ϕ and the incidence angle ψ of the AP and the receiver can be calculated using the rules from

analytical geometry as:

$$\cos\phi = \frac{-\mathbf{d}\cdot\mathbf{n}_{\mathrm{t}}}{\|\mathbf{d}\|}, \tag{4a}$$

$$\cos\psi = \frac{\mathbf{d}\cdot\mathbf{n}_{\mathrm{u}}}{\|\mathbf{d}\|}, \tag{4b}$$

where $\mathbf{n}_{\mathrm{t}} = [0, 0, -1]^{\mathrm{T}}$ and $\mathbf{n}_{\mathrm{u}}$ are the normal vectors at the AP and the receiver planes, respectively and $\mathbf{d}$ denotes the distance vector from the receiver to the AP. The symbols $\cdot$ and $\|\cdot\|$ denote the inner product and the Euclidean norm operators, respectively. Also, $(.)^{\mathrm{T}}$ denotes the transpose operator.

Moreover, the noise at the receiving terminal is drawn from a circularly-symmetric Gaussian distribution of zero mean and variance

$$\sigma_n^2 = \sigma_{sh}^2 + \sigma_{th}^2, \tag{5}$$

where σ_{sh}^2 and σ_{th}^2 are the variances of the shot noise and thermal noise, respectively.

3. Amplitude, Phase and Quadrature (APQ) Modulation

In order to transmit an M-ary modulation signal, we categorize each of the M symbols by three parameters, namely, amplitude, phase and quadrant. Each one of these parameters is represented by a unipolar PAM signal, then the three signals are superimposed in the power domain and transmitted simultaneously. As a result, the circular constellation is transformed into three different linear constellations in order to fit into the constraints of IM/DD. The idea of power domain superposition is based on assigning different power levels for the different signals, so that the receiving terminal can perform SIC and extract and decode each of the three signals separately. Thus, the proposed APQ scheme can be utilized to transmit high order modulations using a single LED and a single PD.

For example, the 16 amplitude and phase-shift keying (APSK) constellation shown in Fig. 2, can be represented by the signals x_1, x_2 and x_3, where x_1 is a 2-PAM signal representing the two possible amplitude levels (i.e., A_1, A_2), x_2 is a 2-PAM signal representing the two possible phase values (i.e., ϕ_1, ϕ_2) and x_3

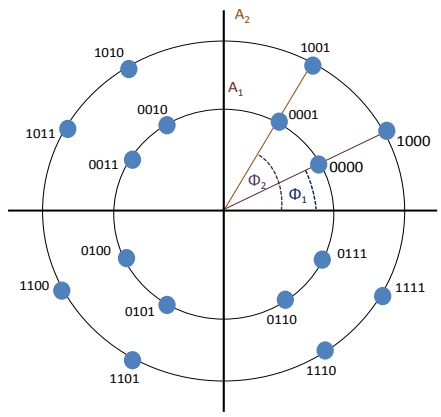

Figure 2: Constellation of 16-Ary APSK.

is a 4-PAM signal representing the four different quadrants of the constellation. An illustration of the APQ encoder is shown in Fig. 3. The three signals are sent simultaneously using the concept of power superposition. In power superposition [22], each signal is assigned a distinct power level, i.e., signal x_i is assigned power level P_i, then the three signals are added and sent as a single signal. To decide on the distinct power levels for the different signals, we implement simple fixed power allocation (FPA) which is typically used in NOMA. In FPA, the power values are calculated as

$$P_{i-1} = \alpha P_i, \tag{6}$$

where $0 < \alpha < 1$ is the power allocation coefficient that determines the power allocated to each signal, i refers to the index of the signal, i.e. $i = 1, 2, 3$, and α satisfies the total power constraint $\sum_{i=1}^{3} P_i = 1$. Consequently, the transmitted signal can be written as

$$x = P_1 x_1 + P_2 x_2 + P_3 x_3. \tag{7}$$

After propagating through the optical channel, the received signal can be expressed as:

$$y = hx = hP_1 x_1 + hP_2 x_2 + hP_3 x_3 + n. \tag{8}$$

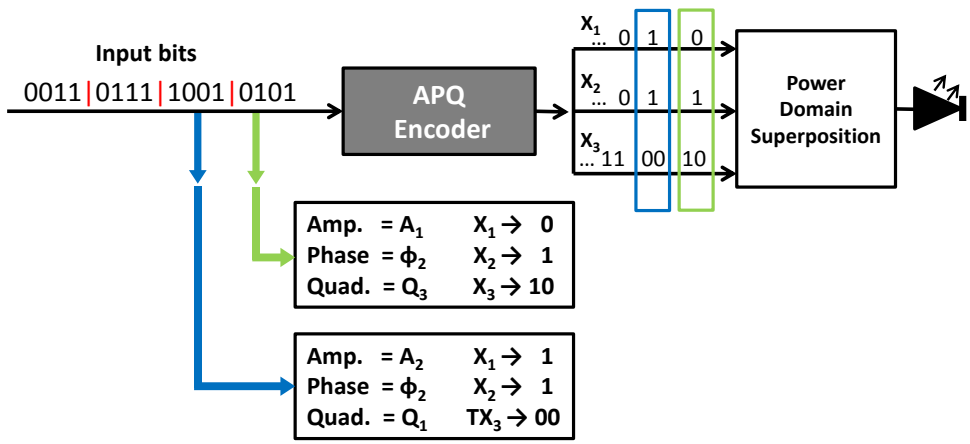

Figure 3: Illustration of APQ Modulation

In order to separate the individual signals at the receiver side, the concept of SIC [23] is used where the signal with the highest power level is decoded first and subtracted to allow for decoding the signals with lower power levels. Given that $P_1 > P_2 + P_3$, the receiver assumes that $hP_2x_2 + hP_3x_3 + n$ is a noise term and decodes x_1. Once x_1 is decoded, it is subtracted from y and the receiver can now decode x_2 assuming that $P_3x_3 + n$ is a noise term. Finally, once x_2 is successfully decoded and subtracted, the remaining part $P_3x_3 + n$ is decoded to get x_3.

It is noted that the complexity of the proposed modulation technique mainly arises at the receiver due to the requirement of performing SIC. However, since the proposed APQ modulation scheme always utilizes three signals to carry the amplitude, phase, and quadrant information, the complexity of SIC does not increase as the modulation order increases.

4. Error Rate Analysis

The symbol error rate (SER) in APQ modulation can be expressed as:

$$\mathrm{Pr} = 1 - \left((1 - \mathrm{Pr}_1) \times (1 - \mathrm{Pr}_2) \times (1 - \mathrm{Pr}_3)\right), \tag{9}$$

where Pr_1, Pr_2 and Pr_3 are the error probabilities in detecting the amplitude, phase and quadrant signals, respectively.

The derivation of the error rate expression depends on the modulation order of each of the individual signals, i.e., x_1, x_2, and x_3. In the following, we derive the error probability for the case of 16-ary APQ modulation. A similar approach can be followed to derive the error probability for different modulation orders once a decision is made on the modulation order of the superimposed signals.

For 16-ary APQ, x_1 and x_2 are represented by 2-PAM signals whereas x_3 is represented by a 4-PAM signal. The error probability in detecting the amplitude signal, x_1, can be written as

$$\begin{aligned}\mathrm{Pr}_1 = &\frac{1}{16}\sum_{i=1}^{2^3} \mathcal{Q}\left(\frac{\gamma h}{\sigma_n}\left(\frac{P_1}{2} - [P_2 P_3][\Delta_{2i}\Delta_{3i}]^T\right)\right) \\ &+ \frac{1}{16}\sum_{i=1}^{2^3} \mathcal{Q}\left(\frac{\gamma h}{\sigma_n}\left(\frac{P_1}{2} + [P_2 P_3][\Delta_{2i}\Delta_{3i}]^T\right)\right),\end{aligned} \tag{10}$$

where $\Delta_2 = [00001111]^T$ and $\Delta_3 = [\delta_1\delta_2\delta_3\delta_4\delta_1\delta_2\delta_3\delta_4]^T$ represent all the possible combinations of the interference caused by x_2 and x_3, respectively and δ_k denotes the power level of the kth level in the 4-PAM signal. After decoding and subtracting x_1, the error probability in detecting the phase signal, x_2, can be written as

$$\mathrm{Pr}_2 = \sum_{e_1=-1,0,1} \mathcal{P}(e_1)\mathrm{Pr}_{2|e1}, \tag{11}$$

where

$$\begin{aligned}\mathrm{Pr}_{2|e1} = &\frac{1}{8}\sum_{i=1}^{2^2} \mathcal{Q}\left(\frac{\gamma h}{\sigma_n}\left(\frac{P_2}{2} - P_3\Delta_3 - e_1 P_1\right)\right) \\ &+ \frac{1}{8}\sum_{i=1}^{2^2} \mathcal{Q}\left(\frac{\gamma h}{\sigma_n}\left(\frac{P_2}{2} + P_3\Delta_3 + e_1 P_1\right)\right),\end{aligned} \tag{12}$$

and

$$\mathcal{P}(e_1) = \begin{cases} 1 - \mathrm{Pr}_1 & e_1 = 0 \\ \frac{1}{2}\mathrm{Pr}_1 & e_i = -1, 1. \end{cases} \tag{13}$$

Its is noted here that e_1 represents the residual interference caused by the detection errors in the first detection stage.

Finally, the error probability in detecting the quadrant signal, x_3, can be written as

$$\mathrm{Pr}_3 = \sum_{e_2=-1,0,1} \sum_{e_1=-1,0,1} \mathcal{P}(e_2|e_1)\mathcal{P}(e_1)\mathrm{Pr}_{3|e_1,e_2}, \tag{14}$$

where

$$\begin{aligned} \mathrm{Pr}_{3|e_1,e_2} = & \frac{3}{4}\mathcal{Q}\left(\frac{\gamma h}{\sigma_n}\left(\frac{P_3}{6} - e_1 P_1 - e_2 P_2\right)\right) \\ & + \frac{3}{4}\mathcal{Q}\left(\frac{\gamma h}{\sigma_n}\left(\frac{P_3}{6} + e_1 P_1 + e_2 P_2\right)\right), \end{aligned} \tag{15}$$

and

$$\mathcal{P}(e_2|e_1) = \begin{cases} 1 - \mathrm{Pr}_{2|e_1} & e_2 = 0 \\ \frac{1}{2}\mathrm{Pr}_{2|e_1} & e_2 = -1, 1. \end{cases} \tag{16}$$

5. Benchmark Model

For the purpose of comparison and evaluation, we implement the optical GSSK scheme. In GSSK, an M-ary modulation scheme is transmitted using a total of $\log_2(M)$ transmitting LEDs. The number and position of the ones and zeros in the symbol to be transmitted determine which groups of LEDs transmits during the symbol duration. To this effect, M different combinations of active and idle LEDs are used to represent the different M constellation symbols. Each LED transmits an on-off keying (OOK) signal, and the channel state information (CSI) available at the receiving terminal is exploited to determine the combination of active LEDs, and thus, the intended symbol. A detailed analysis and performance evaluation of GSSK can be found in [18, 20, 19]. It is worth noting that, GSSK is highly dependent on the channel gain differences of the spatially separated LEDs. Consequently, the existence of similar channel

gains, which is typical in VLC due to the channel symmetry, results in detrimental error performance. In this case, multiple PDs can be used to create channel gain variations at the receiving terminal in order to realize acceptable error performance, as demonstrated in [18]. In order to insure a fair comparison. we assume that both APQ and GSSK use the same power levels in our simulations.

6. Results and Discussions

In this section, we evaluate the performance of the proposed APQ scheme by considering different setup scenarios, which are based on the system model presented in Section 2. The obtained results are compared to the benchmark model presented in Section 5 under the same average power constraints to ensure comparability. We consider a $4 \times 4 \times 3$ m^3 room with a maximum of five high brightness white LEDs and a single PD. We assume that the transmitting LEDs are located at a height of $z = 2.50$ m, while the receiving PDs are placed at a height of $z = 0.75$ m. The used simulation parameters are shown in Table 1, while the front-ends' coordinates are shown in Table 2.

First, we validate the SER expression derived in Section 4. Fig. 4 illustrates that the derived SER expressions agree with simulation results for 16-ary APQ scheme with regard to the transmit signal-to-noise-ratio (SNR). Fig. 5 presents the SER performance for different modulation orders of APQ. It can be noticed that the SER performance deteriorates with increasing M. This can be attributed to the fact that the decision boundaries of M-ary constellation are decreasing when M increases. It is worth mentioning that the performance can be further improved if the power coefficient is optimized. Fig. 5 also shows the performance for different modulation orders of APQ compared to pulse amplitude modulation (PAM). It can be seen from this figure that while PAM provides better error performance for lower modulation orders, the proposed APQ modulation scheme outperforms PAM for higher modulation orders, i.e., 32-ary. This indicates that APQ has the potential to provide reliable commu-

Table 1: Simulation Parameters

Description	**Notation**	**Value**
LED power	P_{LED}	0.25 W
Transmitter semi-angle	φ_i	30°
FOV of the PDs	ϕ_{c_i}	30°
Physical area of PD	A_i	1.0 cm^2
Refractive index of PD lens	n	1.5
Gain of optical filter	$T_s(\phi_{li})$	1.0
Data rate	B	10 Mbps

Table 2: Locations of Transmitting LEDs

LED	**Coordinate**	**PD**	**Coordinate**
Tx1	(2-d,2-d,3)	Rx1	(1,1,0.75)
Tx2	(2+d,2+d,3)	Rx2	(2.1,2.2,0.75)
Tx3	(2,2,3)	Rx3	(2,2,0.75)
Tx4	(2-d,2+d,3)		
Tx5	(2+d,2-d,3)		

nication links when PAM is susceptible to reaching an error floor. Since the channel gain is in the order of 10^{-4}, the corresponding results exhibit an offset of about 80 dB with respect to the SNR at the receiver site. It is shown that the derived analytical results are in excellent agreement with the respective Monte Carlo simulation results.

Next, we examine the SER performance of the proposed APQ scheme, and compare it to the performance of GSSK when the distance between the GSSK transmitters on the x- and y-axis is $d = 1$ m. This setup, adopted in [18], presents a best case scenario for GSSK, as the transmitters are widely spaced resulting in considerable channel gain differences. On the basis of this setup, we simulate the SER performance for various static locations of the receiving PD, i.e., when the PD is located close to the room boundaries, close to the room

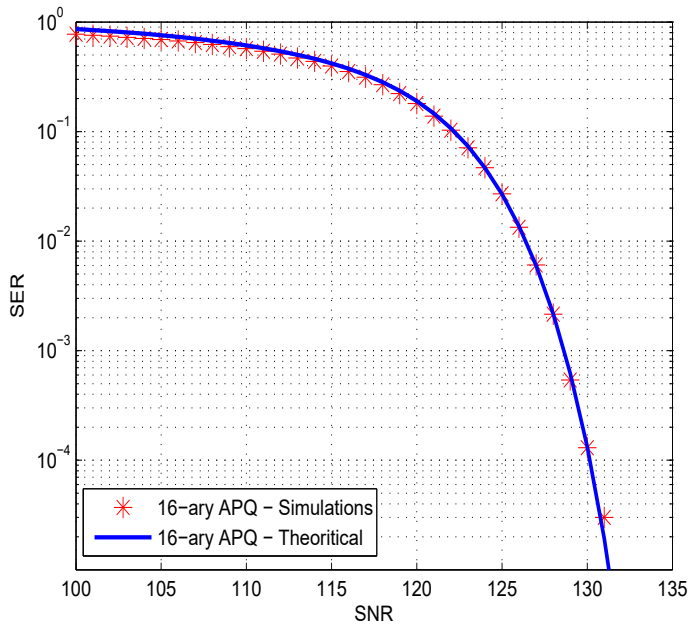

Figure 4: Simulation and Theoretical SER Performance of 16-ary APQ.

center, and exactly in the center of the room. The different locations are denoted by Rx1, Rx2 and Rx3 respectively. Fig. 6 shows that, while GSSK outperforms APQ for the scenario when the receiving PD is located in the proximity of the room center, the proposed APQ scheme provides a good performance regardless of the location of the PD. It is also evident that GSSK fails to provide meaningful communication link when the receiving PD is located in the room center or at the boundaries. This is due to the identical channel gains caused by symmetry, that diminishes the spatial modulation.

Next, we examine the effect of the LEDs' locations on the performance of GSSK. To this end, we simulate the SER for $d = 0.1$ m, which is a typical spacing that has been considered in [24]. Fig. 7 demonstrates the effect of similar channel gains on the performance of GSSK, and shows that the proposed APQ scheme provides superior performance compared to GSSK under the existence of similar channel gains.

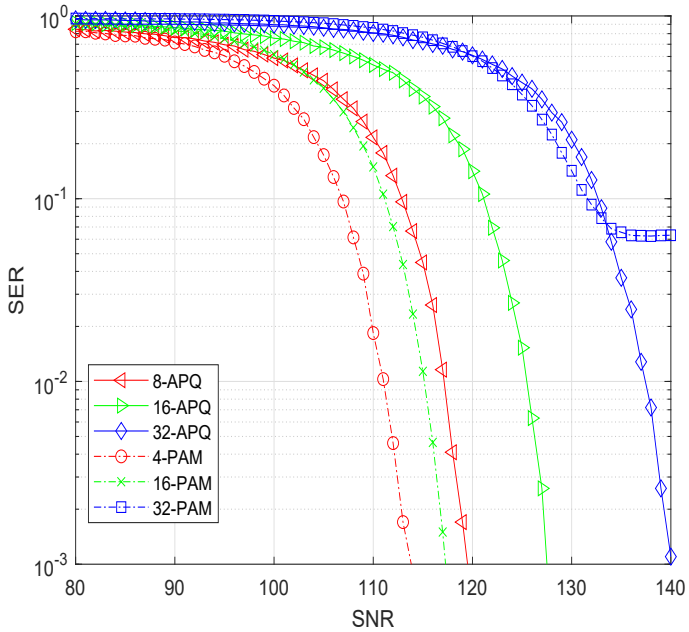

Figure 5: SER Performance vs Transmit SNR for Different Modulation Orders of APQ compared to PAM.

Next, we investigate the achievable system throughput across the simulation area. Fig. 8 and 9 show the normalized achievable throughput for APQ and GSSK for $d = 1$ m and $d = 0.1$ m, respectively. The results are obtained for the case of transmitting 3 bits/symbol, 4 bits/symbol and 5 bits/symbol, under fixed transmit SNR of 130 dB, 140 dB and 150 dB respectively. It is evident that APQ achieves uniform throughput levels across the majority of the simulation area, while a throughput degradation occurs at the boundaries. This is an expected behaviour as the user is receiving from a single LED, which is considered a small cell that serves users within its proximity. On the other hand, GSSK suffers huge throughput non-uniformity due to the similarities between the channel gains observed by the receiving terminal. This throughput non-uniformity hinders the reliability of the communication link, as the user may encounter a substantial performance loss while moving in the coverage area of

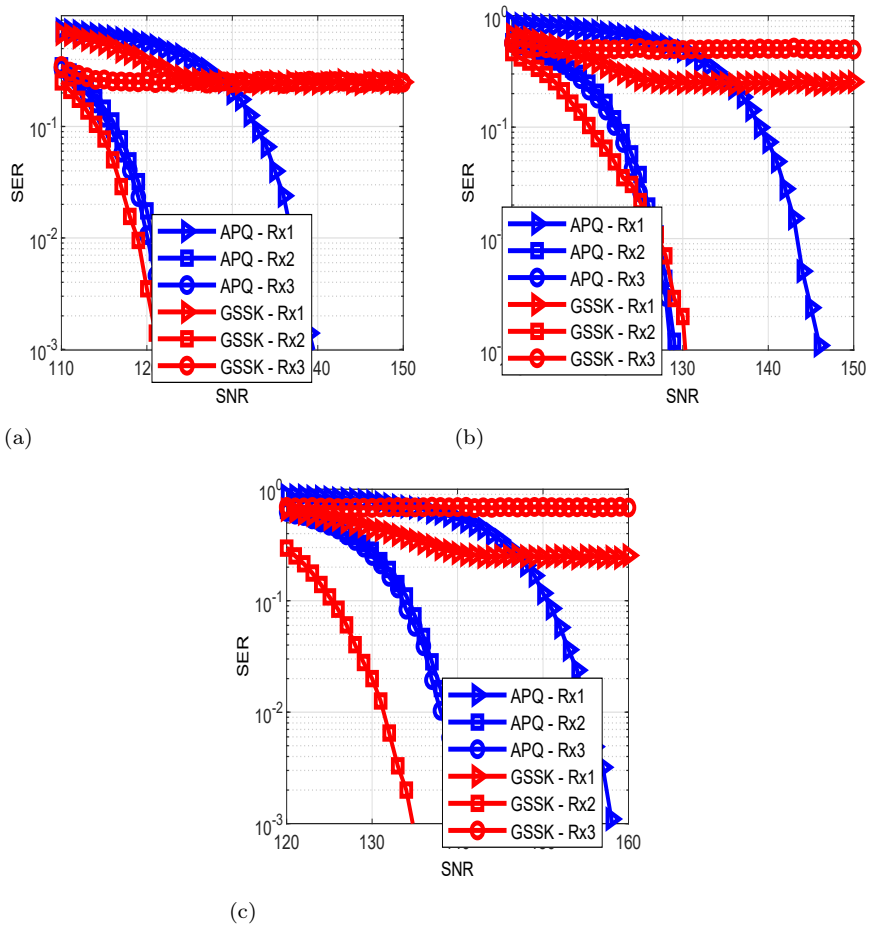

Figure 6: SER vs Transmit SNR for $d = 1$ m (a) 3 bits/symbol, (b) 4 bits/symbol and (c) 5 bits/symbol.

the transmitting LEDs.

7. Conclusions

In this paper, we proposed a novel APQ modulation scheme that is specifically tailored to the requirements imposed by IM/DD based VLC systems. The proposed scheme transmits high order modulation signals by decomposing the amplitude, phase and quadrant information of each symbol, and transmitting

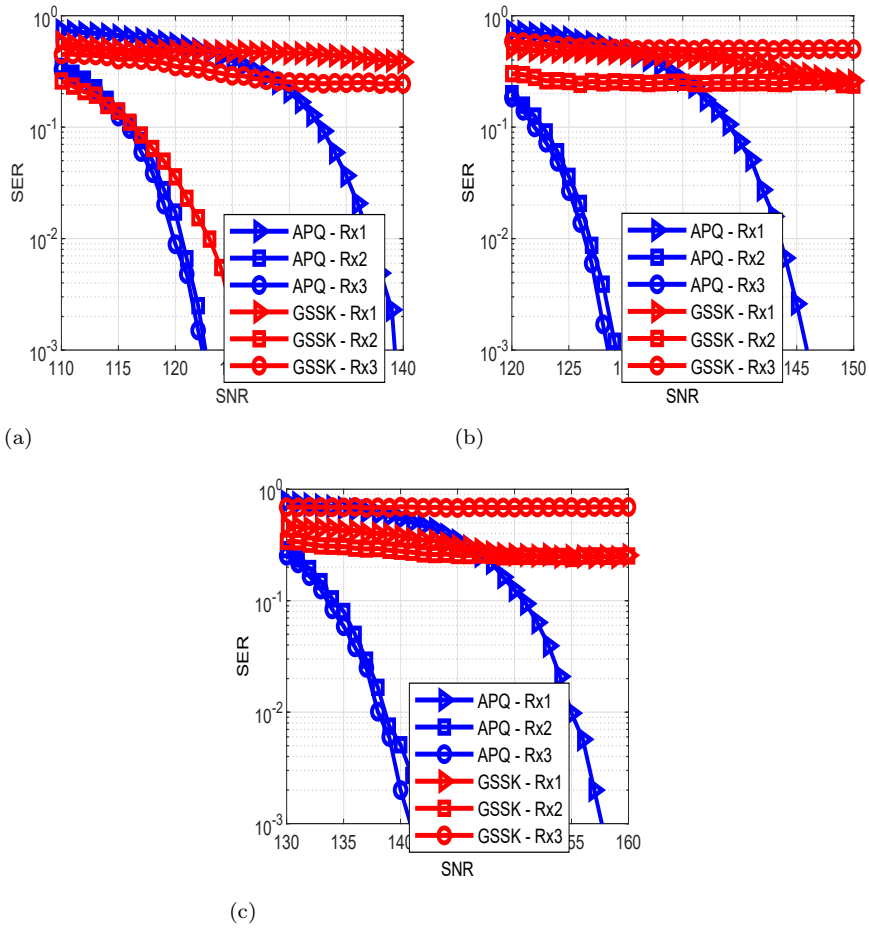

Figure 7: SER vs Transmit SNR for $d = 0.1$ m (a) 3 bits/symbol, (b) 4 bits/symbol and (c) 5 bits/symbol.

the obtained information simultaneously in the power domain. We demonstrated the transmission of 8-ary, 16-ary and 32-ary signals using a single LED and a single photo detector, thus, the proposed APQ scheme provides a cost-effective solution to improve the achievable data rates in indoor VLC systems. On the other hand, GSSK requires N_T transmitting LEDs to transmit a 2^{N_T}-ary signal. Moreover, APQ offers a reliable communication link regardless of the location of the receiving terminal, which makes it suitable for the practi-

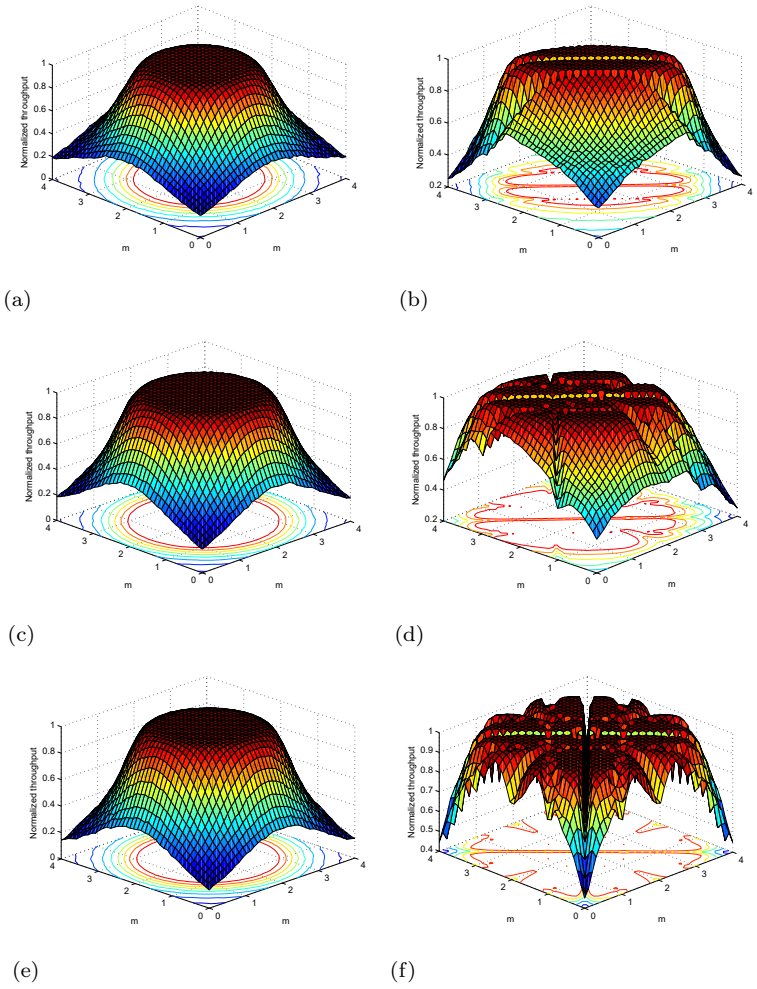

Figure 8: Normalized throughput across the simulation area, $d = 1$ m for (a) APQ 3 bits/symbol, (b) GSSK 3 bits/symbol, (c) APQ 4 bits/symbol, (d) GSSK 4 bits/symbol, (e) APQ 5 bits/symbol, and (f) GSSK 5 bits/symbol.

cal scenarios where the user moves in the proximity of the transmitting LED, while GSSK suffers significant performance degradation when the receiving PD receives similar channel gains from the different transmitting LEDs.

References

[1] H. Haas, L. Yin, Y. Wang, C. Chen, What is LiFi?, J. Lightw. Technol. 34 (6) (2016) 1533–1544.

[2] H. Marshoud, V. M. Kapinas, G. K. Karagiannidis, S. Muhaidat, Non-orthogonal multiple access for visible light communications, IEEE Photon. Technol. Lett. 28 (1) (2016) 51–54.

[3] M. A. Arfaoui, M. D. Soltani, I. Tavakkolnia, A. Ghrayeb, M. Safari, C. Assi, H. Haas, Physical layer security for visible light communication systems: A survey, IEEE Commun. Surveys Tuts. (2020) 1–1.

[4] H. Abumarshoud, H. Alshaer, H. Haas, Dynamic multiple access configuration in intelligent LiFi attocellular access points, IEEE Access 7 (2019) 62126–62141.

[5] D. Zheng, H. Zhang, J. Song, OFDM with differential index modulation for visible light communication, IEEE Photon. J. 12 (1) (2020) 1–8.

[6] A. Ibrahim, T. Ismail, K. Elsayed, M. Saeed Darweesh, J. Prat, Resource allocation and interference management techniques for OFDM-based VLC atto-cells, IEEE Access (2020) 1–1.

[7] H. Zhang, Y. Yuan, W. Xu, PAPR reduction for DCO-OFDM visible light communications via semidefinite relaxation, IEEE Photon. Technol. Lett 26 (17) (2014) 1718–1721. doi:10.1109/LPT.2014.2331360.

[8] M. Zhang, Z. Zhang, An optimum DC-biasing for DCO-OFDM system, IEEE Commun. Lett. 18 (8) (2014) 1351–1354. doi:10.1109/LCOMM.2014.2331068.

[9] J. Tan, Z. Wang, Q. Wang, L. Dai, Near-optimal low-complexity sequence detection for clipped DCO-OFDM, IEEE Photon. Technol. Lett. 28 (3) (2016) 233–236. doi:10.1109/LPT.2015.2493169.

[10] X. Ling, J. Wang, X. Liang, Z. Ding, C. Zhao, Offset and power optimization for DCO-OFDM in visible light communication systems, IEEE Trans. Signal Process 64 (2) (2016) 349–363. doi:10.1109/TSP.2015.2477799.

[11] B. Ranjha, M. Kavehrad, Hybrid asymmetrically clipped OFDM-based IM/DD optical wireless system, IEEE J. Opt. Commun. Netw 6 (4) (2014) 387–396. doi:10.1364/JOCN.6.000387.

[12] F. Yang, J. Gao, S. Liu, Novel visible light communication approach based on hybrid OOK and ACO-OFDM, IEEE Photon. Technol. Lett 28 (14) (2016) 1585–1588. doi:10.1109/LPT.2016.2555620.

[13] S. Dissanayake, K. Panta, J. Armstrong, A novel technique to simultaneously transmit ACO-OFDM and DCO-OFDM in IM/DD systems, in: Proc. IEEE GLOBECOM Workshops (GC Wkshps), 2011, pp. 782–786. doi:10.1109/GLOCOMW.2011.6162561.

[14] D. Tsonev, H. Haas, Avoiding spectral efficiency loss in unipolar OFDM for optical wireless communication, in: Proc. IEEE International Conference on Communications (ICC), 2014, pp. 3336–3341. doi:10.1109/ICC.2014.6883836.

[15] S. Dimitrov, S. Sinanovic, H. Haas, Clipping noise in OFDM-based optical wireless communication systems, IEEE Trans. Commun. 60 (4) (2012) 1072–1081. doi:10.1109/TCOMM.2012.022712.100493.

[16] R. Mesleh, H. Elgala, H. Haas, Optical spatial modulation, IEEE J. Opt. Commun. Netw. 3 (3) (2011) 234–244. doi:10.1364/JOCN.3.000234.

[17] S. Videv, H. Haas, Practical space shift keying VLC system, in: Proc. IEEE Wireless Communications and Networking Conference (WCNC), 2014, pp. 405–409. doi:10.1109/WCNC.2014.6952042.

[18] W. O. Popoola, E. Poves, H. Haas, Error performance of generalised space shift keying for indoor visible light communications, IEEE Trans. Commun. 61 (5) (2013) 1968–1976. doi:10.1109/TCOMM.2013.022713.120501.

[19] Y. Sun, D. K. Borah, E. Curry, Optimal symbol set selection in GSSK visible light wireless communication systems, IEEE Photon. Technol. Lett. 28 (3) (2016) 303–306. doi:10.1109/LPT.2015.2495235.

[20] W. O. Popoola, H. Haas, Demonstration of the merit and limitation of generalised space shift keying for indoor visible light communications, J. Lightw. Technol. 32 (10) (2014) 1960–1965. doi:10.1109/JLT.2014.2310499.

[21] H. Haas, E. Sarbazi, H. Marshoud, J. Fakidis, Chapter 11 - visible-light communications and light fidelity, in: A. E. Willner (Ed.), Optical Fiber Telecommunications VII, Academic Press, 2020, pp. 443–493. doi:https://doi.org/10.1016/B978-0-12-816502-7.00013-0. URL https://www.sciencedirect.com/science/article/pii/B9780128165027000130

[22] H. Marshoud, P. C. Sofotasios, S. Muhaidat, G. K. Karagiannidis, B. S. Sharif, On the performance of visible light communication systems with non-orthogonal multiple access, IEEE Transactions on Wireless Communications 16 (10) (2017) 6350–6364. doi:10.1109/TWC.2017.2722441.

[23] I. Abu Mahady, E. Bedeer, S. Ikki, H. Yanikomeroglu, Sum-rate maximization of noma systems under imperfect successive interference cancellation, IEEE Communications Letters 23 (3) (2019) 474–477. doi:10.1109/LCOMM.2019.2893195.

[24] T. Fath, H. Haas, Performance comparison of mimo techniques for optical wireless communications in indoor environments, IEEE Trans. Commun. 61 (2) (2013) 733–742. doi:10.1109/TCOMM.2012.120512.110578.

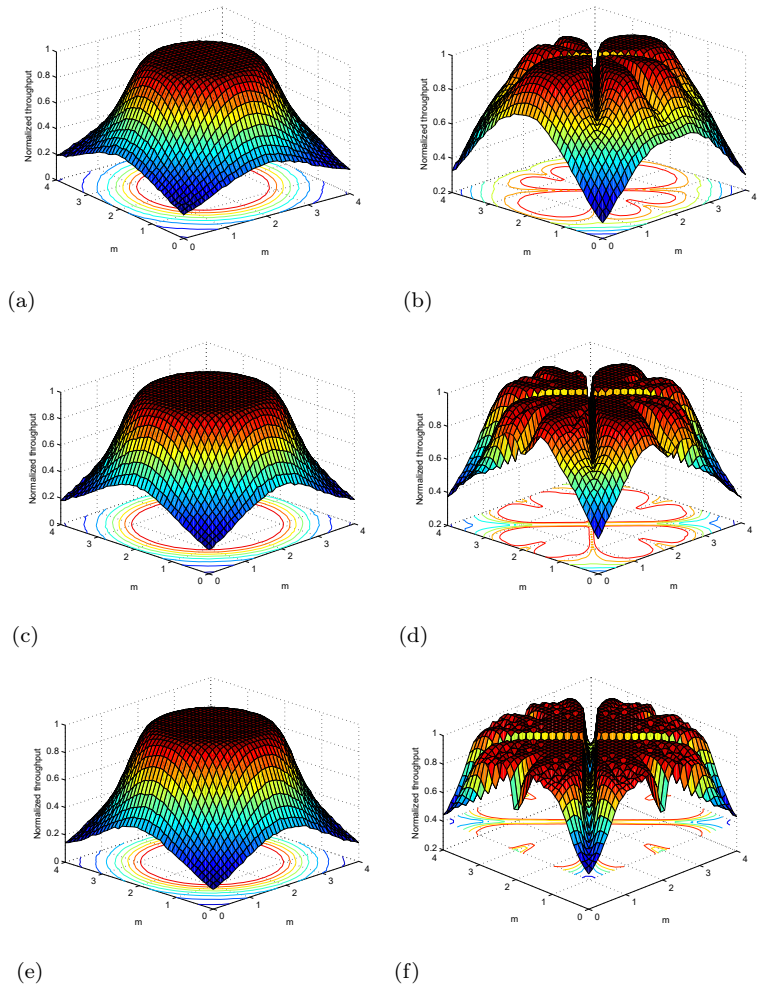

Figure 9: Normalized throughput across the simulation area, $d = 0.1$ m for (a) APQ 3 bits/symbol, (b) GSSK 3 bits/symbol, (c) APQ 4 bits/symbol, (d) GSSK 4 bits/symbol, (e) APQ 5 bits/symbol, and (f) GSSK 5 bits/symbol.